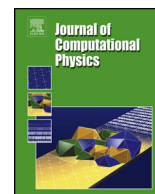


ULRR

Discrete finite volume formulation for multidimensional fragmentation equation and its convergence analysis

Item Type	Article
Authors	Singh, Mehakpreet;Matsoukas, Themis;Ranade, Vivek;Walker, Gavin
Citation	Journal of Computational Physics, 2022, 464, 111368
Publisher	Elsevier
Download date	2026-06-10 12:37:26
Item License	https://creativecommons.org/licenses/by-nc-sa/4.0/
Link to Item	https://doi.org/10.34961/researchrepository-ul.27242109



Discrete finite volume formulation for multidimensional fragmentation equation and its convergence analysis



Mehakpreet Singh^{a,b,*}, Themis Matsoukas^c, Vivek Ranade^a, Gavin Walker^a

^a Bernal Institute, Department of Chemical Sciences, University of Limerick, V94 T9PX Limerick, Ireland

^b Bernal Institute, School of Engineering, University of Limerick, V94 T9PX Limerick, Ireland

^c SH Thomas, Department of Chemical Engineering, Pennsylvania State University, PA 16802, USA

ARTICLE INFO

Article history:

Received 26 August 2021

Received in revised form 27 May 2022

Accepted 31 May 2022

Available online 2 June 2022

Keywords:

Multidimensional fragmentation
Integro-partial differential equation
Finite volume scheme
Monte Carlo method
Population dynamics
Convergence analysis

ABSTRACT

The present work is focused on developing a finite volume scheme for a multidimensional fragmentation equation. The finite volume scheme is established using the concept of overlapping of the cells whose mathematical formulation is both straightforward and robust on any kind of grid. The numerical development is further supported by thorough discussion of the mathematical analysis using Lipschitz condition and consistency of the method. The proposed finite volume scheme conserves the total mass in the system and is shown to estimate several other moments accurately, even though no special measure is taken to capture these moments. The testing of the proposed scheme is investigated against the constant number Monte Carlo method and exact benchmarking problems. The new scheme shows second order convergence on both uniform and nonuniform grids irrespective of the breakage kernel and selection function.

© 2022 The Author(s). Published by Elsevier Inc. This is an open access article under the CC BY license (<http://creativecommons.org/licenses/by/4.0/>).

1. Introduction

Fragmentation is a mechanism in particulate systems that leads to the formation of two or more smaller particles from one bigger particle. It is encountered in industrial and natural settings that involve dispersed solids and granular systems such as depolymerization, colloids, aerosols and crystallizers and in granular processes in general, where it may be the main process of interest (grinding) or an undesirable side effect (i.e., granulation) [1,8,17,41]. The size distribution is governed by the fragmentation equation, an integro-partial differential equation that expresses the balance on the particles formed and destroyed during the processes [9,28,31]. This is often referred to as the one-dimensional fragmentation equation to indicate that it tracks a single state variable, “size”, which is usually taken to be the particle mass. In real settings particles are multicomponent in composition, often characterized by internal porosity, multiple linear dimensions corresponding to different crystallographic facets, and by several other attributes such as surface area, charge etc. Thus the state of the particle must be represented by a multidimensional vector rather than by a single variable. The one-dimensional fragmentation equation has been studied analytically and solutions exist for certain special cases [12,20,33,46,47]. Other studies related to this equation including scaling, convergence, gelation, existence and uniqueness, local and global solutions and steady state solutions can be found in [2,6,14,15,19,22,24,27] and references therein. Much less is available in higher dimensions. A case of binary bicomponent fragmentation was studied by Boyer et al. [7] who obtained the analytic solution with power-law rate of breakage.

* Corresponding author at: Bernal Institute, School of Engineering, University of Limerick, V94 T9PX Limerick, Ireland.
E-mail address: Mehakpreet.Singh@ul.ie (M. Singh).

To formulate the multidimensional problem we notate the state of a particle by the p -dimensional vector $\vec{x} = (x_1, x_2, \dots, x_p) \geq 0$ whose components $x_r, r = 1, \dots, p$ represent independent attributes of the particle state. The size distribution is given by the multidimensional function $f(\vec{x}, t)$ such that $f(\vec{x}, t)d\vec{x}$ is the number of particles in the range $(\vec{x}, \vec{x} + d\vec{x})$. In this work we take x_i to represent the mass of component i in the particle. Accordingly, the sum of all x_r is the total mass Θ of the particle:

$$\Theta(\vec{x}) = \sum_{r=1}^p x_r. \tag{1}$$

The mixed moment of order $(d_1, d_2 \dots d_p)$ is defined

$$\mu_{d_1, d_2, \dots, d_p}(t) = \int_0^\infty \prod_{r=1}^p x_r^{d_r} f(\vec{x}, t) d\vec{x}. \tag{2}$$

The zeroth order moment ($d_r = 0$ for all r) is the total number of particles; the first order moment in position p' and zeroth in all other positions ($d_r = \delta_{r, p'}$) is the mass of component p' , and their sum is the total mass in the system.

The time evolution of distribution f in a multicomponent population undergoing fragmentation is governed by the multidimensional fragmentation equation,

$$\frac{\partial f(\vec{x}, t)}{\partial t} = \int_{\vec{x}}^\infty b(\vec{x}, \vec{y}) S(\vec{y}) f(\vec{y}, t) d\vec{y} - S(\vec{x}) f(\vec{x}, t). \tag{3}$$

Here $S(\vec{x})$ (selection function) is the rate at which particle state \vec{x} produces fragments and $b(\vec{x}, \vec{y})d\vec{x}$ is the number of fragments in the range $(\vec{x}, \vec{x} + d\vec{x})$ produced by state \vec{y} . The integral on the right-hand side of this linear integro-partial differential equation is the rate at which state \vec{x} is produced via fragmentation of particles with larger mass and the second term is its rate of depletion due to fragmentation of state \vec{x} . This equation is to be solved subject to an initial condition $f(\vec{x}, 0) = f_0(\vec{x}) \geq 0$, which is assumed to be known.

The selection function defines the relative fragmentation of different particle sizes and generally depends on all x_r . The breakage function $b(\vec{x}, \vec{y})$ is the marginal distribution of fragments \vec{x} produced from parent state \vec{y} . It is a non negative function that satisfies the following conditions:

$$\int_0^{\vec{y}} b(\vec{x}, \vec{y}) d\vec{x} = \nu(\vec{y}) \geq 2, \quad \forall \vec{y} > 0 \tag{4}$$

$$\int_0^{\vec{x}} \vec{x} b(\vec{x}, \vec{y}) d\vec{x} = \Theta(\vec{y}). \tag{5}$$

The first gives the mean number of fragments produced per fragmentation event; this number must be at least equal to 2, the minimum possible number of fragments. The second condition is a statement of mass conservation and declares that the mass of the fragments is equal to the mass of the parent particle. These conditions are required for physical consistency. In the special case that the number of components p is one the results reverse to the commonly employed one-dimensional fragmentation equation.

Various numerical schemes have been developed to solve the one-dimensional fragmentation equation. They include sectional implementations [37,38], finite element method [5], quadrature method of moments [3,45], finite volume schemes [16,21,29,30,39,43], Galerkin's method [23] and stochastic schemes [4,13,44]. Few numerical methods are available in literature for the multidimensional [10,11,25,34,35,42]. These methods can be only limited for solving the multidimensional fragmentation equation for simpler binary breakage kernel. However, many real life applications related to granulation required the particles to be broken into two or more smaller particles [32].

Sectional methods are highly accurate in predicting number density function and among the most widely used to solve pharmaceutical applications which involve the population balance equations [18,32]. An important element of their implementation is the redistribution of particle properties to neighboring nodes in order to predict accurately the important integral properties of the system (2), in particular, zeroth and first order moments. This results in a formulation that is mathematically complex and computationally expensive.

Finite volume schemes (FVS) are simpler to implement than sectional methods and offer highly accuracy in predicting both number density function and their integral properties [21]. In the standard implementation of FVS particles are assumed to be concentrated at the pivot (mean point) of the cell. As particles are created at different points within a cell, extra effort is required to them back to the pivot, hence adding to the computational cost of the method. Saha et al. [30]

developed two finite volume schemes for solving a multidimensional fragmentation equation based on the assumption that particles are concentrated on the pivots. One scheme implements a single weight to conserve the total mass but the zeroth moment is under predicted. The second method implements two weights and is capable of conserving the zeroth and first order moments but it is not accurate with higher order moments, specifically, μ_{20} and μ_{11} which signifies the total area of particles important for the crystallization applications [26].

Recently, Singh et al. [39] developed a finite volume scheme for the one-dimensional fragmentation equation using the concept of overlapping of cells. The focus of this method was to conserve the total mass in the system, however, predict other integral properties very accurately without any specific measures. Here we generalize this method to arbitrary number of components in order to understand the complete dynamics of the real life application such as granulation and crystallization, not only particle size distribution is important, however the liquid distribution also plays significant role in these applications. The goal is to conserve the total mass while tracking other moments accurately unlike existing schemes that only focused on the zeroth and first order moments [30]. Due to non availability of the analytical solutions of the number density function and their corresponding moments, the numerical results obtained with the new method are compared with a constant number Monte Carlo method with arbitrary fragment size distributions.

The rest of the article is structured as follows: Section 2 is used to derive the new finite volume scheme for approximating a multidimensional fragmentation equation and theoretical results related to the mass conservation are obtained. Next Section 4 consists of numerical results compared with Monte Carlo method and exact results for a two dimensional fragmentation equations. Finally, in Section 5, important conclusions and remarks related this article are made.

2. Formulation of finite volume scheme

We divide the continuous computational domain into $\vec{L} = (L_1, L_2, \dots, L_p)$ discrete cells in p directions with mid points $\vec{x}_i = \frac{\vec{x}_{i+1/2} + \vec{x}_{i-1/2}}{2}$ and step size of the i th $\Delta\vec{x}_i = \vec{x}_{i+1/2} - \vec{x}_{i-1/2}$. The time domain is similarly discretized into $t^{n+1} = t^n + \Delta t^n$ for all $n \in N$. We assume that the average value of f at any time t in i th cell is f_i , which denotes the approximation of the function $f(\vec{x}_i, t)$. If $\wp_i = d\vec{x}$ is the volume of the \mathcal{U}_i cell, the average number density in the cell is

$$f_i = \frac{1}{\wp_i} \int_{\mathcal{U}_i} f(\vec{x}, t) d\vec{x}, \quad i = 1, 2, \dots, L. \tag{6}$$

Using $S_i = S(\vec{x}_i)$ to indicate the value of S in cell i we integrate Eq. (3) over \mathcal{U}_i cell to obtain

$$\frac{df_i}{dt} = B_i - D_i, \tag{7}$$

with B_i and D_i defined as

$$B_i = \frac{1}{\wp_i} \int_{\vec{x}_{i-1/2}}^{\vec{x}_{i+1/2}} \int_{\vec{x}} b(\vec{x}, \vec{y}) S(\vec{y}) f(\vec{y}, t) d\vec{y} d\vec{x}, \tag{8}$$

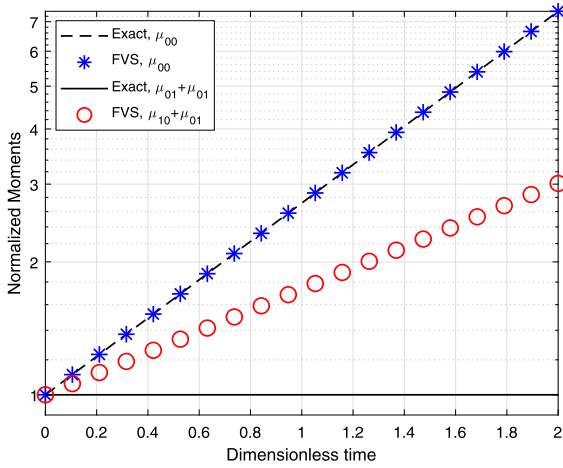
$$D_i = \frac{1}{\wp_i} \int_{\vec{x}_{i-1/2}}^{\vec{x}_{i+1/2}} S(\vec{x}) f(\vec{x}, t) d\vec{x}. \tag{9}$$

Changing the order of integration the birth term, B_i , becomes

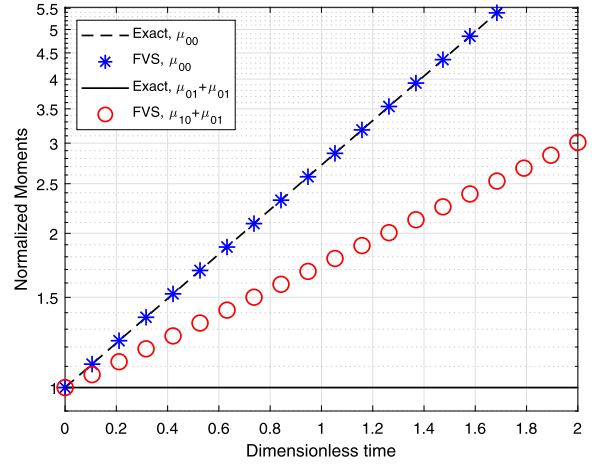
$$B_i = \frac{1}{\wp_i} \left[\int_{\vec{x}_{i-1/2}}^{\vec{x}_{i+1/2}} S(\vec{y}) f(\vec{y}) \int_{\vec{x}_{i-1/2}}^{\vec{y}} b(\vec{x}, \vec{y}) d\vec{x} d\vec{y} + \sum_{k=i+1}^L \int_{\vec{x}_{k-1/2}}^{\vec{x}_{k+1/2}} S(\vec{y}) g(\vec{y}) \int_{\vec{x}_{i-1/2}}^{\vec{x}_{i+1/2}} b(\vec{x}, \vec{y}) d\vec{x} d\vec{y} \right].$$

Applying a midpoint quadrature approximation to the integrals with respect to \vec{x} on right hand side of above equation, leads to the following expression:

$$\begin{aligned} B_i &= \frac{1}{\wp_i} S_i f_i \int_{\vec{x}_{i-1/2}}^{\vec{x}_i} b(\vec{x}, \vec{x}_i) d\vec{x} + \frac{1}{\wp_i \Delta\vec{x}_i} \sum_{k=i+1}^L S_k f_k \Delta\vec{x}_i \int_{\vec{x}_{k-1/2}}^{\vec{x}_{k+1/2}} b(\vec{x}, \vec{x}_i) d\vec{x} + \mathcal{O}(\Delta x^2), \\ &= \frac{1}{\wp_i} \sum_{k=i}^L S_i f_i \int_{\vec{x}_{i-1/2}}^{\rho_k^i} b(\vec{x}, \vec{x}_k) d\vec{x} \end{aligned} \tag{10}$$



(a) Monodisperse initial condition



(b) Exponential initial condition

Fig. 1. Comparison of normalized moments with constant selection function $S(x_1, x_2) = 1$ and breakage kernel $b(x_1, x_2, y_1, y_2) = 2/y_1 y_2$.

On simplification, we have

$$B_i = \frac{1}{\wp_i} \sum_{k=i}^L S_i f_i \eta_{i,k}, \tag{11}$$

where

$$\eta_{i,k} = \int_{\vec{x}_{i-1/2}}^{\rho_k^i} b(\vec{x}, \vec{x}_k) d\vec{x} \quad \text{with} \quad \rho_k^i = \begin{cases} \vec{x}_i, & \text{when } k = i, \\ \vec{x}_{i+1/2}, & \text{otherwise.} \end{cases}$$

In a similar manner, the discretize form of the death term D_i becomes

$$D_i = S_i f_i. \tag{12}$$

Using these results Eq. (7) becomes

$$\frac{df_i}{dt} = \frac{1}{\wp_i} \sum_{k=i}^L S_i f_i \eta_{i,k} - S_i f_i. \tag{13}$$

Using \hat{f}_i to notate the numerical approximation of the number density function f_i over \mathcal{U}_i cell the formulation (13) takes the following form:

$$\frac{d\hat{f}_i}{dt} = \sum_{k=i}^L \eta_{i,k} S_k \hat{f}_k \frac{\wp_k}{\wp_i} - S_i \hat{f}_i. \tag{14}$$

2.1. Zeroth order moment

This formulation conserves the zeroth order moment as proven below. The numerical scheme satisfies the zeroth order moment if it follows the condition

$$\sum_{i=1}^L \frac{d}{dt} \hat{f}_i \wp_i = \sum_{i=1}^L S_k \hat{f}_k \wp_k [v(\vec{x}_i) - 1]. \tag{15}$$

Taking the summation over i on both side of equation (14) we have

$$\sum_{i=1}^L \frac{d\hat{f}_i \wp_i}{dt} = \sum_{i=1}^L \sum_{k=i}^L \eta_{i,k} S_k \hat{f}_k \wp_k - \sum_{i=1}^L \wp_i S_i \hat{f}_i. \tag{16}$$

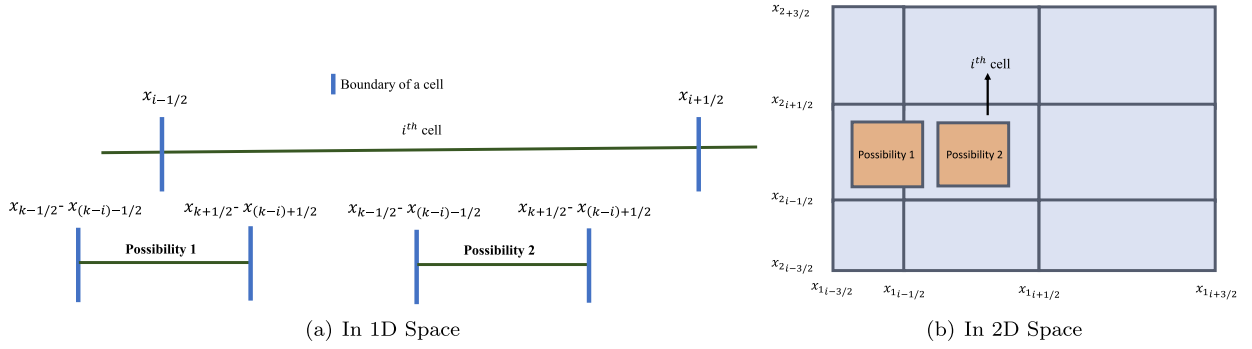


Fig. 2. Depiction of all basic probabilities for overlap.

Changing the order of summations and after some simplifications the result is

$$\sum_{i=1}^L \frac{d\hat{f}_i}{dt} \varphi_i = \sum_{k=1}^L S_k \hat{f}_k \varphi_k \sum_{i=1}^k \eta_{i,k} - \sum_{i=1}^L \varphi_i S_i \hat{f}_i. \tag{17}$$

This implies

$$\sum_{i=1}^L \frac{d\hat{f}_i}{dt} \varphi_i = \sum_{k=1}^L S_k \hat{f}_k \varphi_k \left[\sum_{i=1}^k \eta_{i,k} - 1 \right]. \tag{18}$$

Using the relation (4), finally we have

$$\sum_{i=1}^L \frac{d}{dt} \hat{f}_i \varphi_i = \sum_{i=1}^L S_k \hat{f}_k \varphi_k [v(\vec{x}_i) - 1]. \tag{19}$$

This shows that the formulation (14) holds the zeroth order moment preservation.

While the zeroth moment is tracked accurately, the first moment is not. The proof is given in the Proposition 1) but a simple demonstration is given numerically in Fig. 1 with selection function $S(x_1, x_2) = 1$ and breakage kernel $b(x_1, x_2/y_1, y_2) = 2/y_1 y_2$. The computational grid in this case spans the range $[10^{-8} \ 2]$ comprises of 10×10 cells in two dimensional space. It is clear from this figure that the total mass $\mu_{01} + \mu_{10}$ is underpredicted. In order to achieve the mass conservation, a single weight is added to the formulation without taking into consideration that the particles are concentrated on the representative of the grid. However, the notion of overlapping of cells is used in order to overcome the assumption that particles needs to be concentrated on the representative of the grid.

2.2. Cell overlapping

Let us denote the factor responsible for overlapping of cells by Υ_i^k . For the case of uniform grids, the newly formed particles completely fall (or overlap) inside any cell, hence the value of Υ_i^k is 1. For non-uniform computational domains a particle having properties \vec{x}_k in the cell k th breaks into particles of smaller sizes and falls either in smaller cell than original cell or inside the same cell k . The fragmentation of \vec{x}_k produces two particles \vec{x}_i and \vec{x}_{k-i} and the bounds of the cell where the fragments are formed are $\vec{x}_{i-1/2} = \vec{x}_{k-1/2} - \vec{x}_{(k-i)-1/2}$ and $\vec{x}_{i+1/2} = \vec{x}_{k+1/2} - \vec{x}_{(k-i)+1/2}$. There are two cases to consider:

- **Case 1:** The upper boundary of the domain of the newly born particle falls inside the cell and lower boundary falls outside the cell, that is, $\vec{x}_{i-1/2} > \vec{x}_{k-1/2} - \vec{x}_{(k-i)-1/2}$ and $\vec{x}_{i+1/2} - \vec{x}_{(k-i)+1/2} < \vec{x}_{i+1/2}$.
- **Case 2:** The domain of newly born particle of size $\vec{x}_k - \vec{x}_{k-i}$ falls totally inside the cell, that is, $\vec{x}_{i-1/2} \leq \vec{x}_{k-1/2} - \vec{x}_{(k-i)-1/2}$ and $\vec{x}_{k+1/2} - \vec{x}_{(k-i)+1/2} \leq \vec{x}_{i+1/2}$.

In order to clearly understand the notion of the overlapping of the cells, the schematic representation of all possible cases of overlapping of cells is demonstrated in Fig. 2.

The incorporation of overlapping factor (Υ_i^k) in the equation (7) leads to the following expression:

$$\frac{d\hat{f}_i}{dt} = \sum_{k=i}^L \eta_{i,k} S_k \hat{f}_k \frac{\varphi_k}{\varphi_i} \Upsilon_i^k - S_i \hat{f}_i. \tag{20}$$

Here Υ_i^k is defined as follows:

$$\Upsilon_i^k = \frac{\overline{\wedge}_i^k - \underline{\vee}_i^k}{\Delta \overline{x}_k - \Delta \overline{x}_{k-i}}, \tag{21}$$

where $\overline{\wedge}_i^k = \min(\overline{x}_{i+1/2}, \overline{x}_{k+1/2} - \overline{x}_{(k-i)+1/2})$ and $\underline{\vee}_i^k = \max(\overline{x}_{i-1/2}, \overline{x}_{k-1/2} - \overline{x}_{(k-i)-1/2})$. Here, the terms $\overline{\wedge}_i^k$ and $\underline{\vee}_i^k$ define the bounds of the intersection of the cells k and $(k-i)$ with cell i .

To conserve mass we introduce the weights Φ_i^b and Φ_i^d

$$\Phi_i^b = \frac{1}{\Upsilon_i^k}, \text{ and } \Phi_i^d = \frac{1}{\Theta(\overline{x}_i)} \sum_{i=1}^k \Theta(\overline{x}_k) \eta_{k,i} \tag{22}$$

where $\Phi_1^b = \Phi_1^d = 0$ for particles which falls beyond the lower most boundary and write the fragmentation equation in the form

$$\frac{d\hat{f}_i}{dt} = \underbrace{\sum_{k=i}^L \eta_{i,k} S_k \hat{f}_k \frac{\wp_k}{\wp_i} \Upsilon_i^k \Phi_i^b}_{\hat{B}_i} - \underbrace{S_i \hat{f}_i \Phi_i^d}_{\hat{D}_i} \tag{23}$$

It is worth noting that the weights values considered to be zero beyond the boundaries. This numerical scheme conserves only the total mass in the system (the proof is given below). It will remain to be seen by numerical calculation to what extent this approximation computes the zeroth moment accurately.

2.3. Theoretical proof of mass conservation law and CFL condition

The numerical scheme satisfies mass conservation law if

$$\sum_{i=1}^L \frac{d}{dt} \Theta(\overline{x}_i) \hat{f}_i \wp_i = 0, \text{ where } \Theta(\overline{x}_i) = \sum_{r=1}^p x_{ir}. \tag{24}$$

Proposition 1. *The proposed numerical scheme in Eq. (23) conserves the first order moment, i.e., no mass leaves the computational domain.*

Proof. Multiply Eq. (23) with $\Theta(\overline{x}_i) \wp_i$ on both sides to obtain

$$\sum_{i=1}^L \frac{d\Theta(\overline{x}_i) \hat{f}_i \wp_i}{dt} = \sum_{i=1}^L \sum_{k=i}^L \Theta(\overline{x}_i) \eta_{i,k} \Upsilon_i^k S_k \hat{f}_k \frac{\wp_k}{\wp_i} \Phi_i^b - \sum_{i=1}^L \Theta(\overline{x}_i) \wp_i S_i \hat{f}_i \Phi_i^d. \tag{25}$$

Changing the order of the summation and after simplification we have

$$\sum_{i=1}^L \frac{d\Theta(\overline{x}_i) \hat{f}_i \wp_i}{dt} = \sum_{k=1}^L S_k \hat{f}_k \wp_k \sum_{i=1}^k \Upsilon_i^k \Theta(\overline{x}_i) \eta_{i,k} \Phi_i^b - \sum_{k=1}^L \Theta(\overline{x}_k) \wp_k S_k \hat{f}_k \Phi_k^d, \tag{26}$$

which further simplifies to

$$\sum_{i=1}^L \frac{d\Theta(\overline{x}_i) \hat{f}_i \wp_i}{dt} = \sum_{k=1}^L S_k \hat{f}_k \wp_k \left[\sum_{i=1}^k \Upsilon_i^k \Theta(\overline{x}_i) \eta_{i,k} \Phi_i^b - \Theta(\overline{x}_k) \Phi_k^d \right]. \tag{27}$$

Substituting the values of Φ_i^b and Φ_k^d in Eq. (27) from Eq. (22), we obtain

$$\sum_{i=1}^L \frac{d\Theta(\overline{x}_i) \hat{f}_i \wp_i}{dt} = \sum_{k=1}^L S_k \hat{f}_k \wp_k \left[\sum_{i=1}^k \Upsilon_i^k \Theta(\overline{x}_i) \eta_{i,k} \frac{1}{\Upsilon_i^k} - \Theta(\overline{x}_k) \frac{1}{\Theta(\overline{x}_k)} \sum_{i=1}^k \Theta(\overline{x}_i) \eta_{i,k} \right]. \tag{28}$$

The quantity in square brackets is zero, therefore,

$$\sum_{i=1}^L \frac{d\Theta(\overline{x}_i) \hat{f}_i \wp_i}{dt} = 0. \tag{29}$$

The result states that the first order moment in the computational domain is constant at all times. \square

Since we are developing a numerical method for approximating a generalized fragmentation equation, so it is also important to observe that the numerical solution will always provide non-negative solution. In order to achieve positivity of the solution, some constraints well known as the CFL condition on time step are imposed. Similar to the condition proposed by Singh et al. [36], the following constraint on the time step ensures the positivity of the solution:

$$\Delta t^n < \min_i \left(\left| \frac{\hat{f}_i^n}{\hat{B}_i^n - \hat{D}_i^n} \right| \right). \tag{30}$$

Here \hat{B}_i^n and \hat{D}_i^n are discrete birth and death terms, respectively of the numerical methods described in equation (23).

3. Convergence analysis

The convergence analysis of the finite volume scheme for approximating a multidimensional fragmentation equation is conducted by expresses the equations in vector form. We use \mathbf{f} and $\hat{\mathbf{f}}$ to represent the exact average and numerical values of number density functions, respectively. The vector form of the discrete equation (23) is

$$\frac{\partial \hat{\mathbf{f}}}{\partial t} = \underbrace{\hat{B}_i(\hat{\mathbf{f}}) - \hat{D}_i(\hat{\mathbf{f}})}_{J(\hat{\mathbf{f}})}, \quad \hat{\mathbf{f}}(0) = \mathbf{f}^{in}(0). \tag{31}$$

Here,

$$\hat{B}_i(\hat{\mathbf{f}}) = \sum_{k=i}^L \eta_{i,k} S_k \hat{f}_k \frac{\wp_k}{\wp_i} \Upsilon_i^k \Phi_i^b, \tag{32}$$

$$\hat{D}_i(\hat{\mathbf{f}}) = S_i \hat{f}_i \Phi_i^d. \tag{33}$$

In order to establish our results for Lipschitz condition and convergence, we shall use definitions 3.1–3.2 and Theorem 3.1 of Section 3 listed in Singh et al. [39]. Firstly, the define the norm L^1 considered for convergence as

$$\|\mathbf{f}(t)\| = \sum_{i=1}^L |f_i(t)| \wp_i. \tag{34}$$

3.1. Lipschitz condition

Theorem 1. Assume that the kernels S and b are twice continuously differentiable functions over $]0, \bar{x}_{max}]$ and $C^2(]0, \bar{x}_{max}] \times]0, \bar{x}_{max}]$), respectively. Then there exists a constant

$$G = 2 \max_{\bar{x} \in (0, \bar{x}_{max})} [S(\bar{x})\mu(\bar{x})] < \infty,$$

such that the Lipschitz condition on J is satisfied for all \mathbf{f} and $\hat{\mathbf{f}} \in \mathbb{R}^L$:

$$\|J(\mathbf{f}) - J(\hat{\mathbf{f}})\| \leq G \|\mathbf{f} - \hat{\mathbf{f}}\|. \tag{35}$$

Proof. Using the definition of the norm from Eq. (34) we have

$$\|J(\mathbf{f}) - J(\hat{\mathbf{f}})\| = \sum_{i=1}^L \sum_{k=i}^L \wp_i \eta_{i,k} S_k |f_k - \hat{f}_k| \frac{\wp_k}{\wp_i} \Upsilon_i^k \Phi_i^b + \sum_{i=1}^L \wp_i S_i |f_i - \hat{f}_i| \Phi_i^d.$$

Change the order of the summation and substitute the value of Φ_i^b and Φ_i^d in the above equation to obtain

$$\|J(\mathbf{f}) - J(\hat{\mathbf{f}})\| = \sum_{k=1}^L \Upsilon_i^k S_k |f_k - \hat{f}_k| \wp_k \frac{1}{\Upsilon_i^k} \sum_{i=1}^k \eta_{i,k} + \sum_{i=1}^L \wp_i S_i |f_i - \hat{f}_i| \frac{1}{\Theta(\bar{x}_i)} \sum_{k=1}^i \Theta(\bar{x}_k) \eta_{k,i}. \tag{36}$$

It can be observed that $\frac{\Theta(\bar{x}_k)}{\Theta(\bar{x}_i)} \leq 1 \forall k = 1, 2, \dots, i$ and using this expression

$$\Phi_i^d = \frac{1}{\Theta(\bar{x}_i)} \sum_{k=1}^i \Theta(\bar{x}_k) \eta_{k,i} \leq \frac{\Theta(\bar{x}_i)}{\Theta(\bar{x}_i)} \sum_{k=1}^i \eta_{k,i} = \nu(\bar{x}_i). \tag{37}$$

Using the relation (37), equation (36) becomes

$$\|\mathbf{J}(\mathbf{f}) - \mathbf{J}(\hat{\mathbf{f}})\| \leq \sum_{k=1}^L S_k |f_k - \hat{f}_k| \wp_k \sum_{i=1}^k \eta_{i,k} + \sum_{i=1}^L S_i \wp_i |f_i - \hat{f}_i| \nu(\vec{x}_i). \tag{38}$$

Using $\nu(\vec{x}_k) = \sum_{k=1}^i \eta_{k,i}$ and change $i \rightarrow k$ in second summation, equation (37) can be further simplified to

$$\|\mathbf{J}(\mathbf{f}) - \mathbf{J}(\hat{\mathbf{f}})\| \leq \sum_{k=1}^L S_k |f_k - \hat{f}_k| \wp_k \nu(\vec{x}_k) + \sum_{k=1}^L S_k \wp_k |f_k - \hat{f}_k| \nu(\vec{x}_k) = 2 \sum_{k=1}^L S_k \nu(\vec{x}_k) |f_k - \hat{f}_k| \wp_k. \tag{39}$$

This further implies

$$\|\mathbf{J}(\mathbf{f}) - \mathbf{J}(\hat{\mathbf{f}})\| \leq \sum_{k=1}^L S_k |f_k - \hat{f}_k| \wp_k \nu(\vec{x}_k) + \sum_{k=1}^L S_k \wp_k |f_k - \hat{f}_k| \nu(\vec{x}_k) = 2G \|\mathbf{f} - \hat{\mathbf{f}}\|, \tag{40}$$

where $G = 2 \max_{\vec{x} \in (0, \vec{x}_{max}]}[S(\vec{x})\mu(\vec{x})]$. The relation (40) shows that the Lipschitz constant is independent of \wp and \mathbf{J} clearly satisfy the Lipschitz condition. \square

3.2. Consistency

Our next aim is to prove the main theorem of convergence.

Theorem 2. Suppose that functions $S(\vec{x})$ and $b(\vec{x}|\vec{y})$ are twice continuously differentiable functions over $(0, \vec{x}_{max}]$ and $C^2([0, \vec{x}_{max}] \times]0, \vec{x}_{max}[)$, respectively. Then,

- the solution \hat{f} of the discretization (31) is non-negative, that is, $\hat{f} \geq 0$.
- the discrete formulation (31) is second order consistent, and
- the order of convergence of the proposed finite volume scheme is 2 independently of the type of grid.

Proof. For establishing the above theorem, the necessary conditions which numerical scheme has to follow is the nonnegativity, consistency, and convergence. The nonnegativity of the numerical scheme is given below:

Nonnegativity: For any nonnegative number density $\hat{\mathbf{f}} \in \mathbb{R}^I$ with $\hat{f}_i = 0$ for some $i = 1, 2, \dots, I$. So, Eqs. (32) and (33) give

$$\hat{B}_i(\hat{\mathbf{f}}) \geq 0 \text{ and } \hat{D}_i(\hat{\mathbf{f}}) = 0.$$

This implies $J_i(\hat{\mathbf{f}}) = \hat{B}_i(\hat{\mathbf{f}}) - \hat{D}_i(\hat{\mathbf{f}}) \geq 0 \forall i = 1, 2, \dots, L$, Theorem 3.3 and Theorem 3.4 in Singh et al. [39] imply the nonnegativity of the solution \hat{f} .

Consistency: The i th component of the spatial truncation error (see definition 3.1 in Singh et al. [39]) is

$$\sigma_i(t) = \frac{df_i(t)}{dt} - \frac{d\hat{f}_i(t)}{dt}.$$

Using the Eqs. (11), (12) and (23), the above becomes

$$\frac{df_i(t)}{dt} - J_i(f_i(t)) = B_i - D_i - (\hat{B}_i - \hat{D}_i) = B_i - \hat{B}_i - (D_i - \hat{D}_i). \tag{41}$$

Applying Eqs. (11) and (23) we obtain

$$B_i - \hat{B}_i = \sum_{k=i}^L \eta_{i,k} S_k \hat{f}_k \frac{\wp_k}{\wp_i} - \sum_{k=i}^L \eta_{i,k} \Upsilon_i^k S_k \hat{f}_k \frac{\wp_k}{\wp_i} \Phi_i^b + \mathcal{O}(\Delta \vec{x}^3). \tag{42}$$

Substituting the value of Φ_i^b this becomes

$$B_i - \hat{B}_i = \sum_{k=i}^L \eta_{i,k} S_k \hat{f}_k \frac{\wp_k}{\wp_i} - \sum_{k=i}^L \eta_{i,k} S_k \hat{f}_k \frac{\wp_k}{\wp_i} + \mathcal{O}(\Delta \vec{x}^3). \tag{43}$$

Similar to birth term, consider the $D_i - \hat{D}_i$ term

$$D_i - \hat{D}_i = (1 - \Phi_i^d) S_i f_i + \mathcal{O}(\Delta \vec{x}^3). \tag{44}$$

Table 1
Test problems considered for comparison corresponds to two dimensional fragmentation equation.

Cases	$f(x_1, x_2, 0)$	$b(x_1, x_2 y_1, y_2)$	$S(x_1, x_2)$
1.	$\delta(x_1 - 1)\delta(x_2 - 1)$	$2/(y_1 y_2)$	1
2.	$e^{-x_1 - x_2}$	$2/(y_1 y_2)$	1
3.	$\delta(x_1 - 1)\delta(x_2 - 1)$	$2/(y_1 y_2)$	$x_1 + x_2$
4.	$e^{-x_1 - x_2}$	$2/(y_1 y_2)$	$x_1 + x_2$

Replacing the value of Φ_i^d in the above equation we obtain

$$\begin{aligned}
 D_i - \widehat{D}_i &= \left(1 - \frac{1}{\Theta(\bar{x}_i)} \sum_{i=1}^k \Theta(\bar{x}_k) \eta_{k,i}\right) S_i f_i + \mathcal{O}(\Delta \bar{x}^3), \\
 &= \frac{1}{\Theta(\bar{x}_i)} \left(\Theta(\bar{x}_i) - \sum_{i=1}^k \Theta(\bar{x}_k) \eta_{k,i}\right) S_i f_i + \mathcal{O}(\Delta \bar{x}^3).
 \end{aligned}
 \tag{45}$$

It may be noted that

$$\Theta(\bar{x}_i) = \int_0^{\bar{x}_i} \Theta(\bar{x}) b(\bar{x}, \bar{x}_i) d\bar{x} = \sum_{k=1}^i \int_{\bar{x}_{k-1/2}}^{\rho_i^k} \Theta(\bar{x}) b(\bar{x}, \bar{x}_i) d\bar{x}.$$

Using $\Theta(\bar{x}_i)$ in equation in (45) we obtain

$$D_i - \widehat{D}_i = \frac{1}{\Theta(\bar{x}_i)} \left(\sum_{k=1}^i \int_{\bar{x}_{k-1/2}}^{\rho_i^k} [\Theta(\bar{x}) - \Theta(\bar{x}_k)] b(\bar{x}, \bar{x}_i) d\bar{x} \right) S_i f_i + \mathcal{O}(\Delta \bar{x}^3),$$

which is also written as

$$D_i - \widehat{D}_i = \frac{1}{\Theta(\bar{x}_i)} \left(\sum_{k=1}^{i-1} \int_{\bar{x}_{k-1/2}}^{\bar{x}_{k+1/2}} [\Theta(\bar{x}) - \Theta(\bar{x}_k)] b(\bar{x}, \bar{x}_i) d\bar{x} + \int_{\bar{x}_{i-1/2}}^{\bar{x}_i} [\Theta(\bar{x}) - \Theta(\bar{x}_i)] b(\bar{x}, \bar{x}_i) d\bar{x} \right) S_i f_i + \mathcal{O}(\Delta \bar{x}^3).$$

Using the mid-point approximation on the first integral for $k = 1, 2, \dots, i - 1$ and right-end approximation for second integral in above equation leads numerator equal to $\mathcal{O}(\Delta x^3)$

$$D_i - \widehat{D}_i = \mathcal{O}(\Delta \bar{x}^3).$$

Hence,

$$\sigma_i(t) = \mathcal{O}(\Delta \bar{x}^3) \Rightarrow \|\sigma(t)\| = \mathcal{O}(\Delta \bar{x}^2).$$

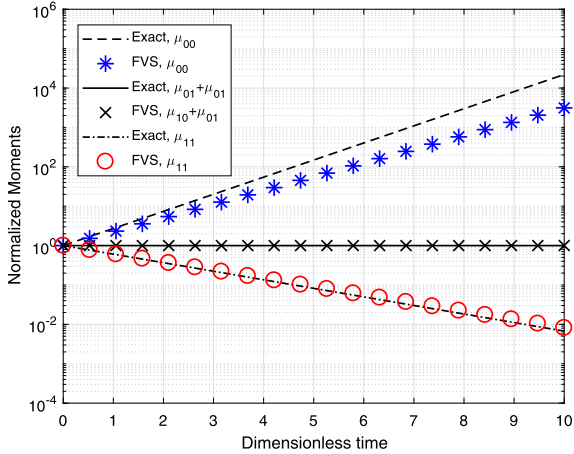
Convergence: Combining Theorem 3.1 of section 3 listed in Singh et al. [40], Theorem 3.3 and the above result on consistency implies that the order of convergence is same as the order of consistency. Therefore, the order of the convergence of the finite volume scheme is 2. \square

4. Numerical results

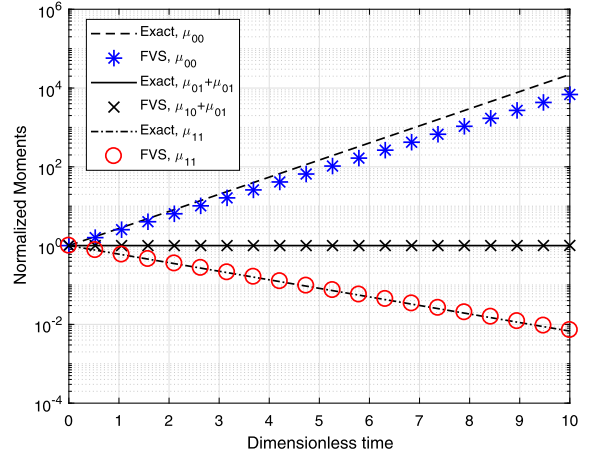
We study the accuracy and computational efficiency of the proposed method through comparison to cases for which analytic results can be obtained. We define the maximum relative errors in moment $\mu_{i,j}$ as

$$\sigma_{i,j} = \left| \frac{\mu_{i,j}^{ana} - \mu_{i,j}^{num}}{\mu_{i,j}^{ana}} \right|
 \tag{46}$$

and use it quantify the accuracy. Here, $\mu_{i,j}^{ana}$ and $\mu_{i,j}^{num}$ denote the analytical and numerical values of respectively. Analytical results are given in Saha et al. [30]. The integration of Eq. (23) is done using MATLAB ODE45 solver on a on machine with specifications is 7300U CPU with 2.70 GHz and 16 GB RAM. The test cases for the various combination of initial conditions, breakage kernels and selection functions for two dimensional studies are summarized in Table 1.

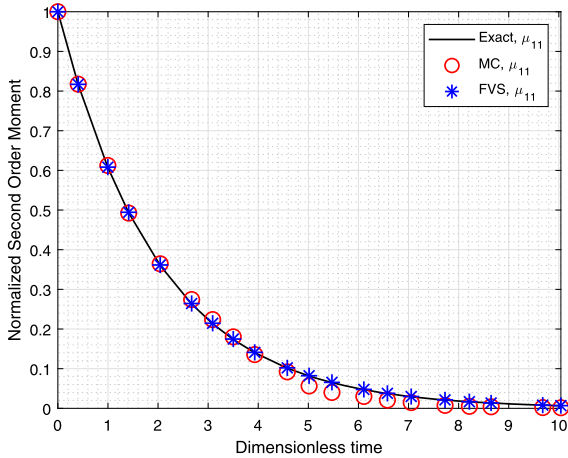


(a) 15×15 grid

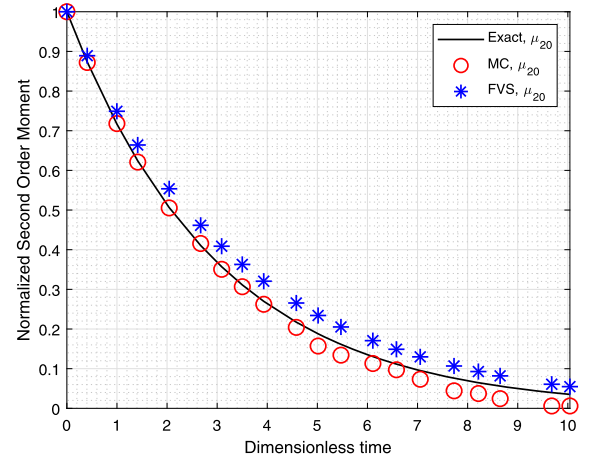


(b) 20×20 grid

Fig. 3. Comparison of various order moments for $f(x_1, x_2, 0) = \delta(x_1 - 1)\delta(x_2 - 1)$, $b(x_1, x_2|y_1, y_2) = 2/y_1 y_2$ and $S(x_1, x_2) = 1$.



(a) Normalized moment μ_{11}



(b) Normalized moment μ_{20}

Fig. 4. Comparison of second order moments obtained using FVS and Monte Carlo (MC) method for $f(x_1, x_2, 0) = \delta(x_1 - 1)\delta(x_2 - 1)$, $b(x_1, x_2|y_1, y_2) = 2/y_1 y_2$ and $S(x_1, x_2) = 1$ for 20×20 grids.

The comparison of numerical results obtained using the finite volume scheme are done against the Monte Carlo (MC) method for which the analytical solutions are not available. The simulation times for MC and FVS are not directly comparable. MC was code in Mathematica and run on a Mac Book Pro (3.1 GHz Dual-Core Intel Core i7) while the FVS simulations were run using 'MATLAB' on 'i5 7300U CPU' with '2.70 GHz' and '16 GB RAM'. The purpose of the MC simulations was to provide a baseline for comparison for those cases that analytic solutions do not exist. As a matter of reference, even though a direct comparison is not appropriate, we note that MC with 200 particles and constant selection function simulated up to $t = 10s$ using acceptance/rejection requires CPU = 0.852 s. We typically average 20 repetitions to obtain smooth results.

4.1. Cases 1 and 2: constant selection function with binary breakage kernel

In both cases 1 and 2 fragmentation is binary with constant selection function (all masses break with the same rate) and each components breaks independently of the other such that its distribution among all fragments produced is uniform. In case 1 the initial condition is monodisperse and in case 2 it is exponential. The monodisperse case produces fragments in the range 0 to 1; the exponential case is more demanding because it produces fragments in the entire range $(0, \infty)$. The computational domain is taken to be from $\bar{x}_{min} = 10^{-9}$ and $\bar{x}_{max} = 2$ and is divided into 15×15 nonuniform cells and are run from time 0 to 10. In order to observe the effect of discretization errors, the numerical simulations are also run for a more refined grid consists of 20×20 nonuniform cells. The MATLAB command for generating the computational grid is provided in Appendix A.

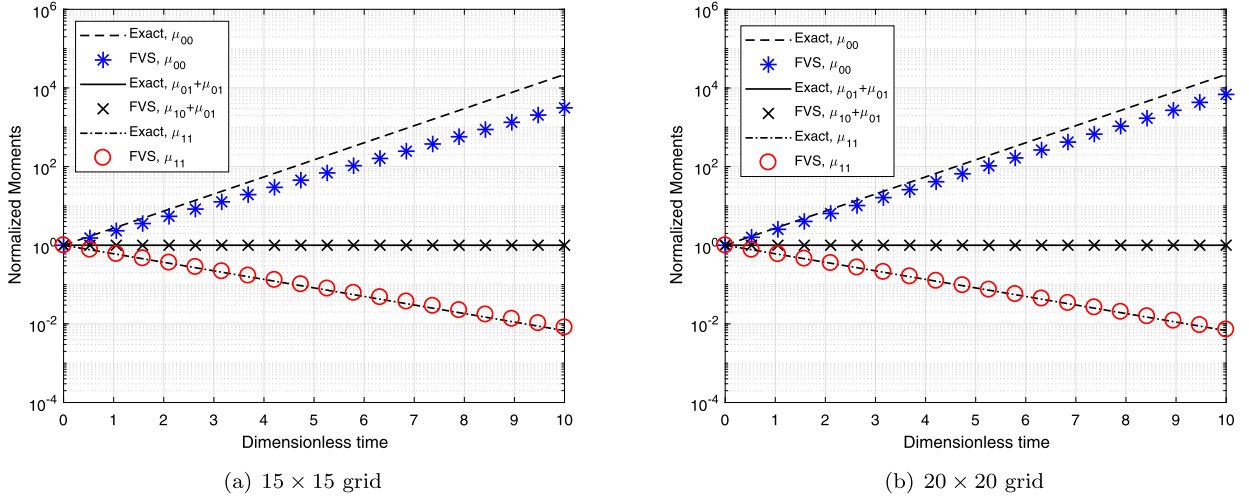


Fig. 5. Comparison of various order moments for $f(x_1, x_2, 0) = e^{-x_1-x_2}$, $b(x_1, x_2, y_1, y_2) = 2/y_1y_2$ and $S(x_1, x_2) = 1$.

Table 2
Relative errors in moments for $f(x_1, x_2, 0) = e^{-x_1-x_2}$, $b(x_1, x_2, y_1, y_2) = \frac{2}{y_1y_2}$ and $S(x_1, x_2) = 1$.

Moments	FVS 15 x 15	FVS 20 x 20	FVS 25 x 25
$\sigma_{0,0}$	0.1784	0.1099	0.0734
$\sigma_{1,0}$	1.9×10^{-7}	1.9×10^{-7}	1.7×10^{-7}
$\sigma_{0,1}$	1.9×10^{-7}	1.9×10^{-7}	1.7×10^{-7}
$\sigma_{1,0} + \sigma_{0,1}$	3.8×10^{-14}	3.8×10^{-7}	3.4×10^{-7}
$\sigma_{1,1}$	0.0092	0.0032	0.0014

Table 3
CPU time for $b(x_1, x_2|y_1, y_2) = \frac{2}{y_1y_2}$ and $S(x_1, x_2) = 1$.

Mesh Points	CPU Time	
	$f(x_1, x_2, 0) = \delta(x_1 - 1)\delta(x_2 - 1)$	$f(x_1, x_2, 0) = e^{-x_1-x_2}$
225	10.47	6.94
400	45.47	42.77
625	270.49	266.45

Results for cases 1 and 2 are provided in Figs. 3 and 5. The simulation is run up to dimensionless time $t = 10$, corresponding to a decrease of the average mass by a factor of $\sim 10^{-4}$ from its initial value. Mass conservation is satisfied during the entire duration of the simulation. The zeroth order moment (number of particles) is underpredicted but the accuracy is improved when more grid points are used. In addition, the mixed order moment is very well approximated by the proposed scheme even with the sparser grid. The second order moments (μ_{11} and μ_{20}) are also compared with analytical solutions and Monte Carlo method as depicted in Fig. 4. Notably, both second order moments are captured with higher accuracy without taking any specific measures for their accuracy. In addition, the average size formed along the x_1 component and total components are compared in Fig. 6 against the Monte Carlo Method and analytical solutions. It shows that the average size particles is computed with very good precision by the FVS and matches well with the Monte Carlo Method and analytical solutions.

The relative errors in the moments obtained using the finite volume scheme are listed in Tables 2 and 4 for different size computational domain. It can be observed that the relative errors in all moments decreased substantially as more refined grid is considered. In terms of computational sense, the finite volume scheme exponential initial condition is highly efficient in computing the different properties as it takes less CPU time than the finite volume scheme with exponential initial condition to calculate these results as depicted in Table 3.

4.2. Cases 3 and 4: linear selection function with binary breakage

In cases 3 and 4 the selection function is linear, i.e., the rate of breakage is proportional to the particle mass and decreases as smaller fragments are formed. The distribution of fragments and the initial conditions are the same as in

Table 4
Relative errors in moments for $f(x_1, x_2, 0) = \delta(x_1 - 1)\delta(x_2 - 1)$, $b(x_1, x_2|y_1, y_2) = \frac{2}{y_1 y_2}$ and $S(x_1, x_2) = 1$.

Moments	FVS	FVS	FVS
	15 × 15	20 × 20	25 × 25
$\sigma_{0,0}$	0.9660	0.8870	0.5187
$\sigma_{1,0}$	3.2×10^{-9}	3.8×10^{-8}	5.7×10^{-9}
$\sigma_{0,1}$	3.2×10^{-9}	3.8×10^{-8}	5.7×10^{-9}
$\sigma_{1,0} + \sigma_{0,1}$	3.9×10^{-4}	7.6×10^{-8}	1.14×10^{-8}
$\sigma_{1,1}$	0.1374	0.0513	0.0231
$\sigma_{2,0}$	0.9796	0.5674	0.1628

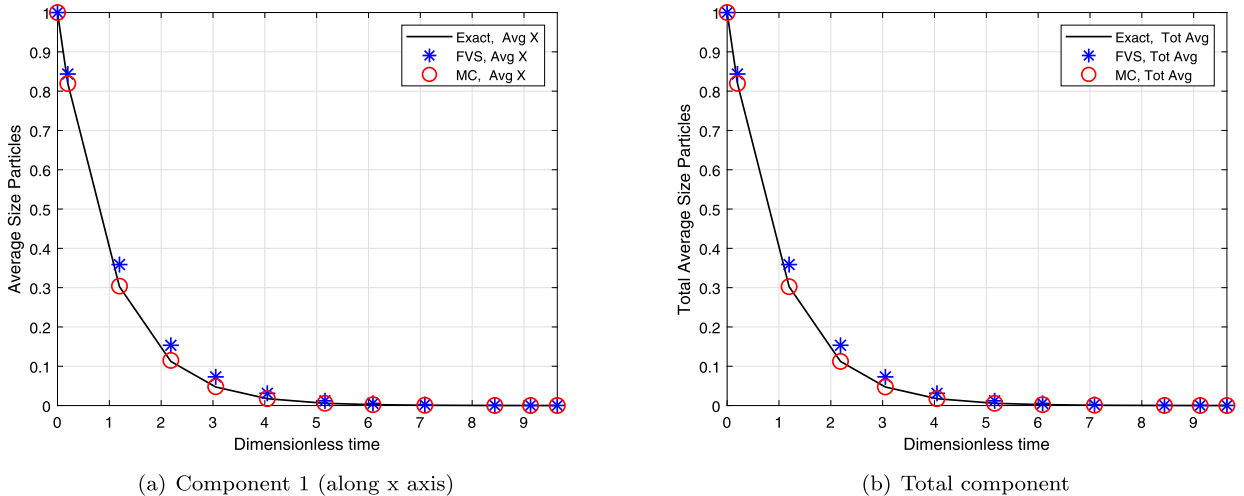


Fig. 6. Comparison of average size particles for $f(x_1, x_2, 0) = \delta(x_1 - 1)\delta(x_2 - 1)$, $b(x_1, x_2|y_1, y_2) = 2/y_1 y_2$ and $S(x_1, x_2) = 1$.

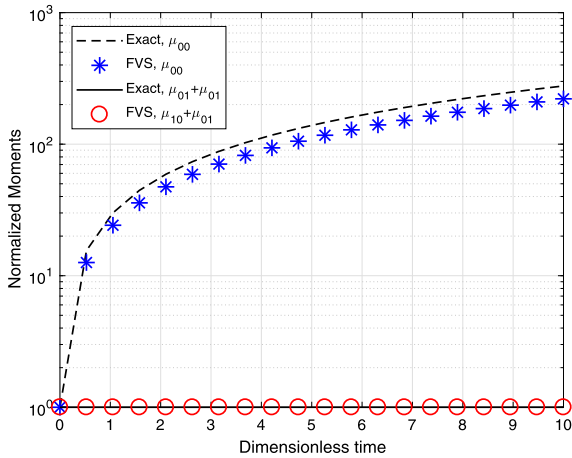
Table 5
Relative errors in moments for $f(x_1, x_2, 0) = \delta(x_1 - 1)\delta(x_2 - 1)$, $b(x_1, x_2, y_1, y_2) = \frac{2}{y_1 y_2}$ and $S(x_1, x_2) = x_1 + x_2$.

Moments	FVS	FVS	FVS
	15 × 15	20 × 20	25 × 25
$\sigma_{0,0}$	0.1997	0.1197	0.0790
$\sigma_{1,0}$	6.5×10^{-6}	3.9×10^{-6}	2.8×10^{-6}
$\sigma_{0,1}$	6.5×10^{-6}	3.9×10^{-6}	2.8×10^{-6}
$\sigma_{1,0} + \sigma_{0,1}$	1.3×10^{-5}	7.8×10^{-6}	5.6×10^{-6}

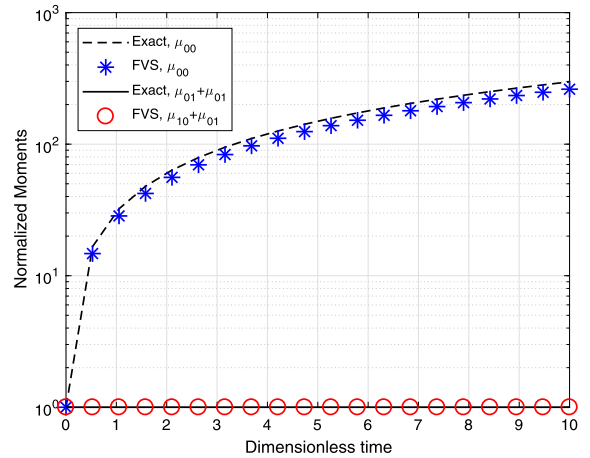
cases 1 and 2. The computational domain is from $\bar{x}_{min} = 10^{-5}$ to $\bar{x}_{max} = 20$ and is divided into 15×15 nonuniform cells. Simulations are run from time $t = 0$ to $t = 10$, which now represents a change of the mean mass by a factor of $\sim 5 \times 10^{-2}$. In contrast to the previous case, it is difficult to obtain the analytical relation for the μ_{11} for these combination of selection function and breakage kernel, hence, the results are compared for zeroth and first order moments and average size of particles formed in the system against the constant number Monte Carlo method.

Results are shown in Fig. 7 for monodisperse initial condition. The zeroth order moment is again underpredicted but by a smaller amount that is decreased when the finer grid is used. Additionally, the second order moments, specifically, μ_{11} and μ_{20} are compared with the Monte Carlo method due to nonavailability of the analytical results. Figures demonstrate that the proposed scheme has the potential to capture these moments very accurately even though no specific measures are taken for their accuracy (refer to Fig. 8). The results for moments associated with the exponential initial condition are identical to those for the monodisperse initial condition. As a result, the comparison has not been addressed, but it has been evaluated in terms of maximum relative errors. Moreover, the average size particle formed in system along x_1 axis and the total average size particle are compared against the Monte Carlo method and analytical solutions in Fig. 9. Results reveal that the proposed scheme is highly accurate and matches well with the Monte Carlo method.

The maximum relative errors in the moments are calculated and listed in Tables 5 and 6 for monodisperse and exponential initial conditions, respectively. In terms of CPU time, the finite volume scheme corresponding to monodisperse initial condition obtained all the numerical results by consuming lesser time than the exponential initial condition (See Table 7).

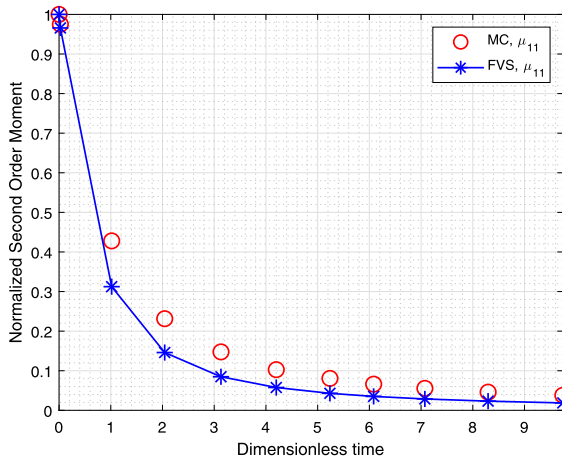


(a) Normalized moments for 15 × 15 grids

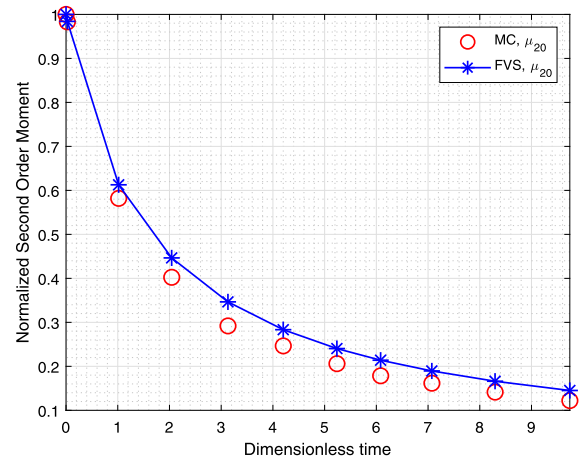


(b) Normalized moments for 20 × 20 grids

Fig. 7. Comparison of various order moments for $f(x_1, x_2, 0) = \delta(x_1 - 1)\delta(x_2 - 1)$, $b(x_1, x_2|y_1, y_2) = 2/y_1 y_2$ and $S(x_1, x_2) = x_1 + x_2$.



(a) Normalized second order moment (μ_{11})



(b) Normalized second order moment (μ_{20})

Fig. 8. Comparison of second order moments obtained using FVS and Monte Carlo (MC) method for $f(x_1, x_2, 0) = \delta(x_1 - 1)\delta(x_2 - 1)$, $b(x_1, x_2, y_1, y_2) = 2/y_1 y_2$ and $S(x_1, x_2) = x_1 + x_2$ for 20 × 20 grids.

Table 6
Relative errors in moments for $f(x_1, x_2, 0) = e^{-x_1-x_2}$, $b(x_1, x_2, y_1, y_2) = \frac{2}{y_1 y_2}$ and $S(x_1, x_2) = x_1 + x_2$.

Moments	FVS 15 × 15	FVS 20 × 20	FVS 25 × 25
$\sigma_{0,0}$	0.1805	0.1073	0.0705
$\sigma_{1,0}$	3.1×10^{-6}	1.6×10^{-6}	1.0×10^{-6}
$\sigma_{0,1}$	3.1×10^{-6}	1.6×10^{-6}	1.0×10^{-6}
$\sigma_{1,0} + \sigma_{0,1}$	6.2×10^{-6}	3.2×10^{-6}	2.0×10^{-6}

Table 7
CPU time for $b(x_1, x_2, y_1, y_2) = \frac{2}{y_1 y_2}$ and $S(x_1, x_2) = x_1 + x_2$.

Mesh Points	CPU Time $f(x_1, x_2, 0) = \delta(x_1 - 1)\delta(x_2 - 1)$	CPU Time $f(x_1, x_2, 0) = e^{-x_1-x_2}$
225	15.59	8.28
400	60.42	49.86
625	313.77	217.40

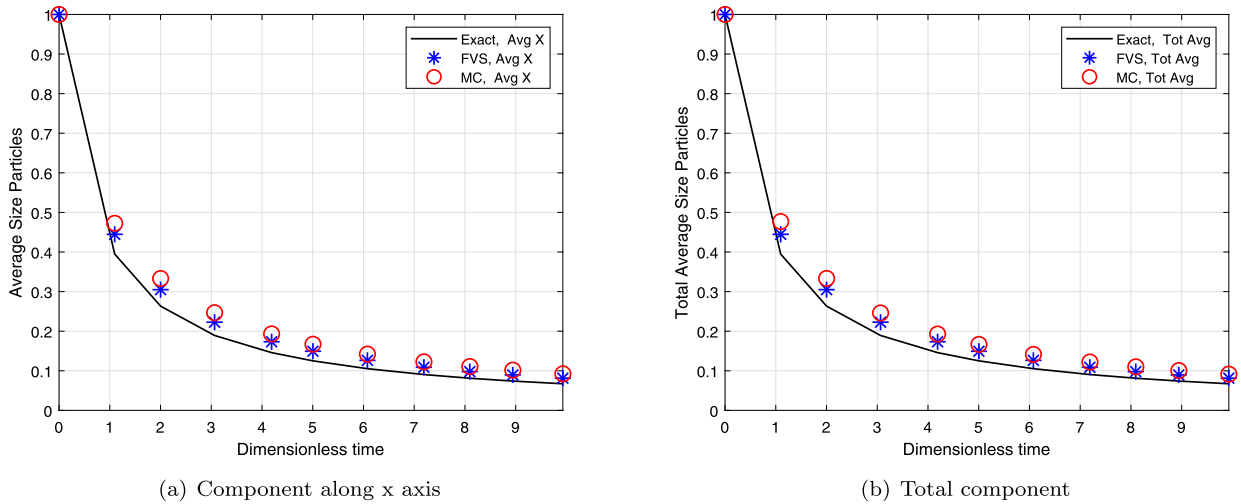


Fig. 9. Comparison of average size particles for $f(x_1, x_2, 0) = \delta(x_1 - 1)\delta(x_2 - 1)$, $b(x_1, x_2, y_1, y_2) = 2/y_1y_2$ and $S(x_1, x_2) = x_1 + x_2$.

5. Conclusions and remarks

A new finite volume approach for approximating a generalized fragmentation equation has been proposed. Key features of the new scheme are a) simpler mathematical formulation, b) robust to apply on any grid, and c) accurate in predicting zeroth and first order moments along with number density function by consuming lesser CPU time. The new scheme has the tendency to compute the second order moments with higher precision on a coarse grid even though no specific measures have been taken for their accuracy. The accuracy and efficiency of the new scheme is measured by considering various selection functions, binary breakage kernel and different initial conditions. It has been also shown that the relative errors in the moments reduced to 50% once a refined grid of 400 nonuniform grid is used for a solving a generalized fragmentation equation. It has been also shown that the new scheme shows second order convergence irrespective of the breakage kernel and selection function corresponding to both uniform and nonuniform grids. Thus the newly developed finite volume scheme is more suitable for solving the real-life problems such as granulation in pharmaceutical industry and grinding of coffee beans in food industry due to its simpler formulation and higher accuracy.

CRediT authorship contribution statement

Mehakpreet Singh: Conceptualization, Methodology, MATLAB Code, Writing – original draft preparation, Investigation, Validation, Writing – reviewing & editing.

Themis Matsoukas: MATHEMATICA Code, Validation, Original draft Preparation, Writing – reviewing & editing.

Vivek Ranade: Investigation, Validation, Writing – reviewing & editing, Supervision.

Gavin Walker: Investigation, Validation, Analyzing the Results, Supervision.

Declaration of competing interest

The authors declare that they have no known competing financial interests or personal relationships that could have appeared to influence the work reported in this paper.

Acknowledgement

The authors gratefully acknowledge the financial support provided by Marie Skłodowska-Curie Individual Fellowship no. 841906 to Dr. Mehakpreet Singh.

Appendix A. Grid generation

Input Values

minimum values of boundaries along x and y -axes = $\{x_{min}, y_{min}\}$,
 maximum values of boundaries along x and y -axes = $\{x_{max}, y_{max}\}$,
 $I = \{I_1 \times I_2\}$ is the number of cells along x and y -axes
 Let us consider x_b and y_b be the boundaries along x and y -axes

Routine for creating boundaries, mean and step size along x -axis

do {
 Commands in MATLAB:
 $x_b = \exp[\text{linspace}(\ln(x_{min}), \ln(x_{max}), I_1)]$ where linspace is a MATLAB function
 $x_m = 0.5(x_b(i+1) + x_b(i))$ is a mean of the cell along x -axis
 $\Delta x_m = x_b(i+1) - x_b(i)$ is the step size along x -axis

Routine for creating boundaries, mean and step size along y -axis

do {
 Commands in MATLAB:
 $y_b = \exp[\text{linspace}(\ln(y_{min}), \ln(y_{max}), I_2)]$ where linspace is a MATLAB function
 $y_m = 0.5(y_b(i+1) + y_b(i))$ is a mean of the cell along y -axis
 $\Delta y_m = y_b(i+1) - y_b(i)$ is the step size along y -axis

References

- [1] F. Ahamed, M. Singh, H.S. Song, P. Doshi, C.W. Ooi, Y.K. Ho, On the use of sectional techniques for the solution of depolymerization population balances: results on a discrete-continuous mesh, *Adv. Powder Technol.* 31 (2020) 2669–2679.
- [2] H. Amann, C. Walker, Local and global strong solutions to continuous coagulation–fragmentation equations with diffusion, *J. Differ. Equ.* 218 (2005) 159–186.
- [3] M.M. Attarakih, H.J. Bart, N.M. Faqir, Numerical solution of the bivariate population balance equation for the interacting hydrodynamics and mass transfer in liquid–liquid extraction columns, *Chem. Eng. Sci.* 61 (2006) 113–123.
- [4] S. Bhoi, D. Sarkar, Hybrid finite volume and Monte Carlo method for solving multi-dimensional population balance equations in crystallization processes, *Chem. Eng. Sci.* 217 (2020) 115511.
- [5] Y. Bie, X. Cui, Z. Li, A coupling approach of state-based peridynamics with node-based smoothed finite element method, *Comput. Methods Appl. Mech. Eng.* 331 (2018) 675–700.
- [6] J.P. Bourgade, F. Filbet, Convergence of a finite volume scheme for coagulation–fragmentation equations, *Math. Comput.* 77 (2008) 851–882.
- [7] D. Boyer, G. Tarjus, P. Viot, Exact solution and multifractal analysis of a multivariable fragmentation model, *J. Phys.* 17 (1997) 13–38.
- [8] A. Braumann, M. Kraft, W. Wagner, Numerical study of a stochastic particle algorithm solving a multidimensional population balance model for high shear granulation, *J. Comput. Phys.* 229 (2010) 7672–7691.
- [9] J. Bridgewater, Particle technology, *Chem. Eng. Sci.* 50 (1995) 4081–4089.
- [10] A. Buffo, V. Alopaeus, Solution of bivariate population balance equations with high-order moment-conserving method of classes, *Comput. Chem. Eng.* 87 (2016) 111–124.
- [11] A. Buffo, M. Jama, V. Alopaeus, Liquid–liquid extraction in a rotating disc column: solution of 2d population balance with HMMC, *Chem. Eng. Res. Des.* 115 (2016) 270–281.
- [12] P. Dubovskii, V. Galkin, I. Stewart, Exact solutions for the coagulation–fragmentation equation, *J. Phys. A, Math. Gen.* 25 (1992) 4737.
- [13] A. Eibeck, W. Wagner, An efficient stochastic algorithm for studying coagulation dynamics and gelation phenomena, *SIAM J. Sci. Comput.* 22 (2000) 802–821.
- [14] A. Eibeck, W. Wagner, Stochastic particle approximations for Smoluchowski’s coagulation equation, *Ann. Appl. Probab.* 11 (2001) 1137–1165.
- [15] M. Escobedo, P. Laurençot, S. Mischler, B. Perthame, Gelation and mass conservation in coagulation–fragmentation models, *J. Differ. Equ.* 195 (2003) 143–174.
- [16] F. Filbet, P. Laurençot, Numerical simulation of the Smoluchowski coagulation equation, *SIAM J. Sci. Comput.* 25 (2004) 2004–2028.
- [17] Y.K. Ho, C. Kirse, H. Briesen, M. Singh, C.H. Chan, K.W. Kow, Towards improved predictions for the enzymatic chain-end scission of natural polymers by population balances: the need for a non-classical rate kernel, *Chem. Eng. Sci.* 176 (2018) 329–342.
- [18] H.Y. Ismail, S. Shirazian, M. Singh, D. Whitaker, A.B. Albadarin, G.M. Walker, Compartmental approach for modelling twin-screw granulation using population balances, *Int. J. Pharm.* 576 (2020) 118737.
- [19] I. Jeon, Existence of gelling solutions for coagulation–fragmentation equations, *Commun. Math. Phys.* 194 (1998) 541–567.
- [20] G. Kaur, R. Singh, M. Singh, J. Kumar, T. Matsoukas, Analytical approach for solving population balances: a homotopy perturbation method, *J. Phys. A, Math. Theor.* 52 (2019) 385201.
- [21] J. Kumar, J. Saha, E. Tsotsas, Development and convergence analysis of a finite volume scheme for solving breakage equation, *SIAM J. Numer. Anal.* 53 (2015) 1672–1689.
- [22] P. Laurençot, C. Walker, Steady states for a coagulation–fragmentation equation with volume scattering, *SIAM J. Math. Anal.* 37 (2005) 531–548.
- [23] H. Liu, R. Gröpler, G. Warnecke, A high order positivity preserving dg method for coagulation–fragmentation equations, *SIAM J. Sci. Comput.* 41 (2019) B448–B465.
- [24] D. McLaughlin, W. Lamb, A. McBride, An existence and uniqueness result for a coagulation and multiple-fragmentation equation, *SIAM J. Math. Anal.* 28 (1997) 1173–1190.
- [25] M.N. Nandanwar, S. Kumar, A new discretization of space for the solution of multi-dimensional population balance equations: simultaneous breakup and aggregation of particles, *Chem. Eng. Sci.* 63 (2008) 3988–3997.
- [26] H.M. Omar, S. Rohani, Crystal population balance formulation and solution methods: a review, *Cryst. Growth Des.* 17 (2017) 4028–4041.
- [27] B. Perthame, L. Ryzhik, Exponential decay for the fragmentation or cell-division equation, *J. Differ. Equ.* 210 (2005) 155–177.
- [28] M.J. Rhodes, *Introduction to Particle Technology*, John Wiley & Sons, 2008.
- [29] J. Saha, A. Bück, Conservative finite volume schemes for multidimensional fragmentation problems, *Mathematics* 9 (2021) 635.
- [30] J. Saha, N. Das, J. Kumar, A. Bück, Numerical solutions for multidimensional fragmentation problems using finite volume methods, *Kinet. Relat. Models* 12 (2018) 79.
- [31] A.D. Salman, M. Hounslow, J.P. Seville, *Granulation*, Elsevier, 2006.
- [32] S. Shirazian, H.Y. Ismail, M. Singh, R. Shaikh, D.M. Coker, G.M. Walker, Multi-dimensional population balance modelling of pharmaceutical formulations for continuous twin-screw wet granulation: determination of liquid distribution, *Int. J. Pharm.* 566 (2019) 352–360.
- [33] R. Simha, On the degradation of branched chain molecules, *J. Chem. Phys.* 24 (1956) 796–802.
- [34] M. Singh, Accurate and efficient approximations for generalized population balances incorporating coagulation and fragmentation, *J. Comput. Phys.* 435 (2021) 110215.
- [35] M. Singh, New finite volume approach for multidimensional Smoluchowski equation on nonuniform grids, *Stud. Appl. Math.* 147 (2021) 955–977.
- [36] M. Singh, H.Y. Ismail, T. Matsoukas, A.B. Albadarin, G. Walker, Mass-based finite volume scheme for aggregation, growth and nucleation population balance equation, *Proc. R. Soc. A, Math. Phys. Eng. Sci.* 475 (2019) 20190552.

- [37] M. Singh, G. Kaur, T. De Beer, I. Nopens, Solution of bivariate aggregation population balance equation: a comparative study, *React. Kinet. Mech. Catal.* 123 (2018) 385–401.
- [38] M. Singh, J. Kumar, A. Bück, E. Tsotsas, An improved and efficient finite volume scheme for bivariate aggregation population balance equation, *J. Comput. Appl. Math.* 308 (2016) 83–97.
- [39] M. Singh, T. Matsoukas, A.B. Albadarin, G. Walker, New volume consistent approximation for binary breakage population balance equation and its convergence analysis, *ESAIM: Math. Model. Numer. Anal.* 53 (2019) 1695–1713.
- [40] M. Singh, T. Matsoukas, G. Walker, Mathematical analysis of finite volume preserving scheme for nonlinear Smoluchowski equation, *Phys. D: Nonlinear Phenom.* 402 (2020) 132221.
- [41] M. Singh, S. Shirazian, V. Ranade, G.M. Walker, A. Kumar, Challenges and opportunities in modelling wet granulation in pharmaceutical industry—a critical review, *Powder Technol.* (2022) 117380.
- [42] M. Singh, K. Vuik, G. Kaur, H.J. Bart, Effect of different discretizations on the numerical solution of 2d aggregation population balance equation, *Powder Technol.* 342 (2019) 972–984.
- [43] M. Singh, G. Walker, V.V. Ranade, Formulation and convergence analysis of new methods for reduced fragmentation model: illustrative application to depolymerization, *ESAIM: Math. Model. Numer. Anal.* 56 (2022) 943–967.
- [44] J. Wei, Comparison of computational efficiency of inverse and acceptance–rejection scheme by Monte Carlo methods for particle coagulation on cpu and GPU, *Powder Technol.* 268 (2014) 420–423.
- [45] S. Wu, E.K. Yapp, J. Akroyd, S. Mosbach, R. Xu, W. Yang, M. Kraft, Extension of moment projection method to the fragmentation process, *J. Comput. Phys.* 335 (2017) 516–534.
- [46] R.M. Ziff, New solutions to the fragmentation equation, *J. Phys. A, Math. Gen.* 24 (1991) 2821.
- [47] R.M. Ziff, E. McGrady, The kinetics of cluster fragmentation and depolymerisation, *J. Phys. A, Math. Gen.* 18 (1985) 3027.